Biometals (2021) 34:1313–1328
https://doi.org/10.1007/s10534-021-00344-7

Ecofriendly preparation of silver nanoparticles-based nanocomposite stabilized by polysaccharides with antibacterial, antifungal and antiviral activities

Mohamed Hasanin · Mostafa A. Elbahnasawy · Amr M. Shehabeldine · Amr H. Hashem

Received: 18 June 2021 / Accepted: 13 September 2021 / Published online: 25 September 2021

Abstract In the present work, sustainable and green method was used to prepare silver nanoparticles (Ag-NPs), followed with incorporation into tertiary nanocomposite consisted of starch, oxidized cellulose and ethyl cellulose. The prepared tertiary silver-nanocomposite (Ag-NC) was fully characterized via instrumental analysis (UV-vis, FT-IR, XRD, SEM, EDX and TEM) and evaluated for antibacterial, antifungal, and antiviral activities. Ag-NC significantly suppressed growth of tested bacterial strains (*Escherichia coli*, *Pseudomonas aeruginosa*, *Staphylococcus aureus* and *Bacillus subtilis*) as compared with controls. Antifungal activity revealed that the prepared tertiary Ag-NC has a promising antifungal activity towards unicellular *(Candida albicans) and multicellular fungi (Aspergillus niger, A. terreus, A. flavus* and *A. fumigatus)*. In same line, both Ag-NC and free Ag-NPs have shown a dose-dependent reduction in Vero cell line with maximum non-toxic dose at 6.25 and 12.5 µg/mL, respectively. Both Ag-NPs and Ag-NC exhibited antiviral effects against Herpes simplex virus, Adenovirus and Coxsackie B virus in a dose-dependent manner. Combined treatment of Ag-NPs incorporated into tertiary nanocomposite based on starch, oxidized cellulose and ethyl cellulose opens new possibilities to be more efficient nanomaterials for preventing microbial growth. In conclusion, the prepared tertiary Ag-NC has a promising antibacterial, antifungal as well as antiviral activities.

Keywords Nanocomposite · Silver nanoparticles · *Bacillus cereus* · Antimicrobial activity · Antifungal activity · Antiviral activity

M. Hasanin
Cellulose and Paper Department, National Research Centre, Dokki, Cairo 12622, Egypt

M. A. Elbahnasawy (✉) · A. M. Shehabeldine (✉) · A. H. Hashem
Botany and Microbiology Department, Faculty of Science, Al-Azhar University, 11884 Cairo, Egypt
e-mail: mostafa.elbahnasawy@azhar.edu.eg

A. M. Shehabeldine
e-mail: dramrshehab@azhar.edu.eg

Introduction

Due to the inappropriate use of conventional antibiotics, new strains of bacteria have emerged with increased levels of resistance and have shown a wide distributed to community-associated bacteria, leading to global public health problems (Abo-State et al. 2012; Ezzat et al. 2014). There have been efforts from various scientific fields to find solutions that may contribute to alleviate this problem. In this context, the search for antimicrobial substances has become a current and important goal in materials science (Dhingra et al. 2020; Shehabeldine et al. 2020). The development of polymer-based nanocomposites with

antimicrobial activity offers interesting possibilities because the polymer matrix can be varied in order to meet not only specific technological requirements but also nanostructures with size and shape dependent properties that can be exploited (Xue et al. 2020). Microbial-based biosynthesis of NPs is advantageous compared to chemical and physical methods due to its non-toxic, environmentally friendly, cost-effective and more stable nature (Bhavya et al. 2021). Biogenic Ag-NPs have received great attention due to their biological, physical, chemical, and antimicrobial properties (Yaqoob et al. 2020). Biological synthesis of Ag-NPs includes bacteria, fungi, algae and plant (Hashem et al. 2021a; Jogaiah et al. 2019; Konappa et al. 2021; Nayak et al. 2020). Currently, there is also an urgent need to develop bio-nanocomposites that can control or inhibit pathogenic microbes by incorporating nanoparticles with known antibacterial activity in or enhancing the antibacterial properties that the polymer matrix already possesses. A number of previous studies have reported numerous investigations of the use of metallic nanoparticles as an antimicrobial agent (Elbahnasawy et al. 2021a; Hashem et al. 2021b). The intrinsic biological properties of these materials depend on several factors such as the mineral involved, particle size, structure, and surface area. All possible combinations of these factors can help delay antimicrobial resistance (Makvandi et al. 2020).

Fungal infections significantly increased in the last two decades, with high rates of mortality, especially in immunodeficiency patients (Chang et al. 2017). Pathogenic fungi invade more than 1.2 billion individuals overall the world with at least 1.7 million deaths/year (Campoy and Adrio 2017; Chang et al. 2017; GAFFI). Invasive fungal infections for human are candidiasis and aspergillosis (Schmiedel and Zimmerli 2016). The recent annual incidence of invasive aspergillosis, candidiasis, and mucormycosis is over 300,000, 750,000, and 10,000 cases, respectively (Bongomin et al. 2017).

The main important of composite materials is localized in the stabilization nanoparticles. It is well known that the colloidal nanoparticle suspensions usually unstable. Consequently, needs of incorporation of nanometals into stabilized and regulation system is obligate. The polysaccharides are the preferred group of polymers which used in these systems (Abu-Elghait et al. 2021; Dacrory et al. 2021; Elsayed et al. 2021; Hasanin et al. 2021a, 2021b; Youssef et al. 2021). In addition, starch is one of the edible available biopolymer. TEMPO oxide cellulose is one of nanocellulose fibers which functionalized using 2,2,6,6-tetramethylpiperidine-1-oxyl radical (TEMPO). Ethyl cellulose is the ether cellulose derivate. Virus infections continue to pose significant global health challenges. With the recent viral outbreaks, including coronavirus, influenza, Ebola and dengue, there is utmost and urgent need for novel effective antivirals. Recently, Ag-NPs have introduced as an alternative antiviral to overcome the development of drug resistance to conventional antivirals. Ag-NPs are emerging as one of the easiest options for the control of viral diseases due to their extraordinary antiviral activity in a broad-spectrum way. Several reports have confirmed the robust antiviral effect of Ag-NPs against numerous human pathogenic viruses such as Human immunodeficiency virus type 1 (HIV-1), Herpes simplex virus type 1 and type 2 (HSV-1 and HSV-2), Respiratory syncytial virus (RSV), adenovirus, Influenza virus, parainfluenza virus, Tacaribe virus (TCRV), Monkeypox virus (MPV), Hepatitis B virus (HBV), Norovirus, Coxsackievirus, Chikungunya, Dengue, Poliovirus, Rift Valley fever virus, Vaccinia virus (VACV), SARS-CoV-2 (Jeremiah et al. 2020; Chen et al. 2013; Maduray and Parboosing 2020). In this study, new compensation between three biopolymers was carried out to improve the efficiency of Ag-NPs as antimicrobial and antiviral.

Materials and methods

Materials

Starch (St), and ethyl cellulose (EC) were purchased from Sigma-Aldrich. TOC was prepared according to our previous work (Hasanin and Moustafa 2020). Other chemicals, culture media and reagents used in this study were purchased from Modern Lab Co., India in analytical grade without any purification required.

Microbial strains and growth conditions

Escherichia coli (ATCC 25922), *Pseudomonas aeruginosa* (ATCC 27853), *Staphylococcus aureus* (ATCC23235), and *Bacillus subtilis*

(ATCC23857) were cultivated in Luria–Bertani (LB) broth medium (1% tryptone, 0.5% yeast extract, 1% NaCl, pH 7). Unicellular (*Candida albicans* ATCC90028) and multicellular fungi (*Aspergillus niger* RCMB 02724, *A.terreus* RCMB 02574, *A. flavus* RCMB 02782 and *A. fumigatus* RCMB 02568) were obtained from the Regional Center of Mycology and Biotechnology, Al-Azhar university, Cairo, Egypt. Fungal strains were inoculated on malt extract agar (MEA) plates then incubated for 3–5 days at 28 ± 2 °C, and then kept at 4 °C for further use (Hashem et al. 2020; Khalil and Hashem 2018).

Bacterial Strain isolation and identification

The bacterial strain used in this work was isolated from soil samples (taken from a depth of 5–10 cm) collected from the eastern desert of Egypt (Latitude: 29° 58′ 49.06″ N and longitude: 32° 7′ 3.39″ E). The strain was isolated by serial dilution plate technique onto LB agar plates (1% tryptone, 0.5% yeast extract, 1% NaCl, 1.5% agar and pH 7) at 37 °C. For molecular identification, genomic DNA was extracted and amplified for 16S-rDNA using the specific 16S-rDNA primers 27F (5′-AGAGTTTGATCCTGGCT-CAG-3′) and 1492R (5-GGTTACCTTGTTAC-GACTT-3′). PCR products were purified by pure link quick gel extraction kit (Elbahnasawy et al. 2020) and sequenced using same primers by ABI 3730xl DNA sequencer (GATC Biotech, Germany). The sequence consensus was compared with NCBI Gene Bank data base using the NCBI BLAST program. Phylogenetic analyses were performed using the neighbour-joining method based on 1000 replicates using MEGA 7.0 software (Elbahnasawy et al. 2021b).

Biosynthesis of Ag-NPs

Ag-NPs were prepared as described previously (El-Nahhal et al 2020). In brief, Cell-free extract (CFE) was obtained from overnight-grown bacterial isolate strain and used in fabrication of Ag-NPs from their precursor $AgNO_3$ (1 mM). Formation of Ag-NPs was monitored visually by turning brown reaction with reference to the controls and confirmed by UV–visible spectrophotometer (scanning spectra range of 300–700 nm).

Preparation of Ag-NPs nanocomposite

The Ag-NPs loaded nanocomposite (Ag-NC) was prepared using a green method in which Ag-NPs were loaded using solvent phase exchange. In brief, both of TOC and St were dispersed in deionized water with concentration of 1% (wt/vol) for each component. Biosynthesized Ag-NPs (0.5 g) were added to the mixture (100 ml) under steering at 1500 rpm for 1 h. EC (100 ml) was first dissolved in ethanol as 1% (wt/vol), then added to the mixture and followed by steering overnight. The reaction mixture was concentrated to half volume in vacuum oven at 70 °C. Any precipitates were filtrated and washed by methanol two times then washed by deionized water and preserved in refrigerator to further investigations.

Characterizations of Ag-NC

UV–visible spectroscopy (UV–vis) spectra of the prepared Ag-NPs and Ag-NC were measured on V-630 UV–vis spectrophotometer (Jasco, Japan) in the range of 300–700 nm. The Ag-NC and its component were characterized using FT-IR spectrometer (Nicolet Impact-400 FT-IR spectrophotometer) in the range of 400–4000 cm^{-1} using KBr method (0.002 g sample was grinded with 0.98 g KBr) using Spectrum Two IR Spectrometer – Perk in Elmer, Inc., Shelton, USA. The X-Ray diffraction (XRD) of Ag-NC and its component were investigated on a Diano X-ray diffractometer using Cu-Kα radiation source energized at 45 kV and a Philips X-ray diffractometer (PW 1930 generator, PW 1820 goniometer) with Cu-Kα radiation source (λ = 0.15418 nm) XRD Model diffractometer, Shimadzu 7000, Japan. The topographical study was carried out using scanning electron microscopy (SEM) with energy dispersive electron spectroscopy (EDX) Model FEI IN SPECTS Company, Philips, Holland, environmental scanning without coating. The surface morphology of Ag-NPs and Ag-NC was carried out using JEOL 1010 transmission electron microscopy (TEM), Model JEM2010, Japan. The samples were processed according to (Shehabeldine et al. 2021a; Elbahnasawy et al. 2021a).

Antifungal activity

The antifungal activity of Ag-NC, Ag-NPs, $AgNO_3$, Nystatin were evaluated using agar well-diffusion. Fungal suspensions of *C. albicans* ATCC 90028, *A. niger* RCMB 02724, *A. terreus* RCMB 02574, *A. flavus* RCMB 02782, and *A. fumigatus* RCMB 02568 were prepared in sterilized phosphate buffer solution (PBS) pH 7.0, and then the inoculums was adjusted to 10^7 spores/ mL after counting in a cell counter chamber. One mL of each fungal suspension was uniformly distributed onto MEA Plates. Sterile Cork-borer was used for making wells (8 mm) in inoculated MEA plates, and 100 µL of the tested compounds at concentration 10 mg/mL was added. All MEA plates were incubated at 30 °C for 72 h, and then the inhibition zone diameters were measured.

Antibacterial activity

The antibacterial activities of Ag-NC, Ag-NPs, $AgNO_3$, and Amikacin were evaluated using paper disk assay (El-Zayat et al. 2021).Bacterial suspensions of either *E. coli* (ATCC 25922), *P. aeruginosa* (ATCC 27853), *S. aureus* (ATCC23235), or *B. subtilis* (ATCC23857) were spread onto the plates Mueller–Hinton agar plates. Paper disks (7 mm in diameter) preloaded by 50 µl of either Ag-NC, Ag-NPs, $AgNO_3$ or Amikacin were put on agar plates. Plates were incubated at 35 ± 2 °C for 24 h. The diameters of the inhibition zone, representing the antibacterial activity, were measured edge-to-edge across the center of the disk. Microorganisms showing a clear zone of more than 12 mm were inhibited. All tested compounds (50 µL each) were loaded into paper disks in triplicates.

Minimum inhibitory concentration

Antibacterial and antifungal activities of Ag-NC and Ag-NPs were tested by using of standard microdilution method which enables to determine the minimum inhibition concentration (MIC) of antimicrobial substances. The MIC value express a minimum concentration of a tested compound that inhibited the growth of tested bacteria and fungi. MICs of Ag-NC, Ag-NPs, Nystatin (for fungi), and Amikacin (for bacteria) were determined using different concentrations (10–160 µg/ml) for each compound (Balouiri et al. 2016). Determination of MIC was carried out on microtitration plates employing a method when we tested a dispersion of Ag-NC 2-to-128 times, in the geometrical progression, diluted by addition of 100 mL of the Mueller–Hinton cultivation medium inoculated by tested bacterial and fungal strain at a concentration of 10^5e10^6 CFU mL^{-1}. The minimum bactericidal/fungicidal concentration (MBC and MFC) was calculated by plating out samples of the MIC and the next two higher concentrations onto LB agar for tested bacteria and MEA for tested fungi. The lowest concentration that resulted in no colony growth on LB and MEA was determined to be the MBC and MFC.

Cytotoxicity assay

The in vitro cytotoxic activity of Ag-NC and Ag-NPs was determined against kidney epithelial cells derived from African green monkey called Vero cells (ATCC CCL-81) followed our previous protocol (Shehabeldine et al. 2021b). Vero cells were cultured in DMEM supplemented with L-glutamine (2.9 mg/mL), penicillin–streptomycin, and 10% fetal calf serum. At 90% confluence, the cells were harvested using 0.25% trypsin EDTA at 37 °C. Aliquots of Vero containing 1×10^5 cells was pipetted into a 96-well flat-bottomed plate and incubated at 37 °C for 24 h. Next, Vero cells were treated with two-fold serial dilutions of Ag-NC or Ag-NPs (3.125, 6.25, 12.5, 25, 50, 100, 200, 400 and 800 µg/mL) followed by incubation for 24 h at 37 °C. Untreated cells were included as a control. The cytotoxicity was quantitatively evaluated by using MTT (3-(4,5-dimethylthiazolyl-2)-2,5-diphenyltetrazolium bromide) colorimetric assay. In brief, overnight-grown Vero cells were washed three times by PBS and followed by addition of the yellow tetrazolium MTT solution (100 µL each well) for 2 h at 37 °C for reduction of MTT by metabolites of active cells. Following this incubation, DMSO (100 µL each well) was added and the plate was placed on shaker (150 rpm, 5 min) to thoroughly mix the formazan into the solvent. Optical density (OD) of each well was then measured at 560 nm and subtract background at 620 nm by using a microplate reader. Each experiment was performed in triplicate and the relative cellular viability percentage was calculated as a percentage to untreated control cells (cell viability (%) = (treated cells absorbance − blank absorbance)/(untreated

cells absorbance − blank absorbance) × 100), while the inhibition percentage was calculates as follows, inhibition (%) = 100 − cell viability (%). The cytotoxic concentration$_{50}$ (CC_{50}) is the concentration of compounds which exert half of its maximal inhibitory effect and inhibit 50% of cell growth. CC_{50} was estimated by a straight line (linear regression) model. The maximum non-toxic dose (MNTD) of each compound was determined and used for further antiviral studies.

Antiviral activity

The inhibitory effect of Ag-NC and Ag-NPs was determined against Herpes simplex virus (HSV-1), Adenovirus (Adeno) and Coxsackie B virus 2 (CoxB2) using the MTT assay. Overnight-grown Vero cells in 96-well plates were infected with a mixture containing HSV-1 or Adeno, or CoxB2 pretreated with equal volume (1:1 v/v) Ag-NC (3.12, 6.25, 12.5 µg/mL) or Ag-NPs (1.56, 3.12, 6.25 µg/mL) for 24 h. After shaking (150 rpm) for 5 min, the plates were incubated (37 °C, 5% CO_2) for one day to allow the virus to take effect (Hamouda et al. 2021). The cells were washed and added to DMEM medium (2% FBS) and then incubated (37 °C, 5% CO_2) for 48 h. Cellular viability was detected at OD_{560} nm and the antiviral effects were observed using inverted microscope examination.

Results and discussion

Isolation and identification of the bacterial isolate

Out of bacterial isolates, strain MAE 16 has shown potent capabilities to fabricate Ag-NPs. Strain MAE 16 was further identified to the species level. Cells were shown to be gram-positive, endospore formers, motile, rods and arranged in pairs or chains. Genetically, 16S rRNA sequence (924 bp) was subjected to NCBI BLAST analysis and the neighbor-joining phylogenetic tree indicated that MAE 16 formed a clade with species members of the *Bacillus (B.)* genus (Fig. 1A). MAE 16 has shared the highest level of sequence similarity (98%) with *B. cereus* strains including, *B. cer*eus SZL35, *B. cer*eus LB-2, *B. cer*eus NIOER178, *B. cer*eus FMC-3, *B. cer*eus SJ 25, and *B. cer*eus GZUB38. Accordingly, strain MAE 16 was identified as *B. cer*eus strain MAE 16 and its 16S rRNA sequence was deposited at the NCBI with a received accession number MN049485. It well known that Ag-NPs have characteristic optical properties in the visible light spectrum. The CFE of *B. cer*eus MAE 16 has shown a rapid formation of Ag-NPs which was visually observed by turning reaction color to dark brown within few hours of exposure to the precursor silver nitrate. Excitation of surface plasmon excitation (SPR) is a characteristic spectroscopic signature of Ag-NPs formation and the color change of reaction is attributed to the SPR excitation (Shehabeldine et al. 2021a; Elbahnasawy et al. 2021a). Ag-NPs exhibited SPR with an intense absorption peak at 430 nm in UV–vis spectra range after 24 h of incubation with 1 mM $AgNO_3$ (Fig. 1B).

Characterizations of Ag-NPs

FTIR analysis

FTIR spectroscopic analysis was used to evaluate the functional groups which remark in the molecules after and before composition. Figure 2 illustrates the FTIR spectra of Ag-NPs, St, TEMPO, EC and Ag-NC. Ag-NPs spectrum contain the main function groups band which mainly referred to the neat bacterial medium extract. The bands at 3225, 2924, 1600, 1374, 1035 and 509 cm^{-1} which corresponding for hydroxyl group, CH stretching vibrations of CH_3 and CH_2, secondary amine NH Stretch, Vinyl CH bend, for C–O of glucose ring (Singh et al. 2013). Moreover, the small peak at 779 cm^{-1} and sharp peak at 509 cm^{-1} represent the reduction of silver to Ag-NPs. Otherwise, the composite materials contain the main functional groups as assigned in the literatures as well as our previous work. Starch spectrum contains the main characteristics bands which referred to neat starch which in agreement with our previozus works (Abu-Elghait et al. 2021; Shehabeldine and Hasanin 2019) at 3437, 2932, 1641 and 1026 cm^{-1} corresponding for hydroxyl group starching vibration, CH group starching vibration, binding adsorbed water and CO of glucose unite, respectively. In addition, TEMPO presented the characteristics bands at 3440, 2928, 1746 and 1636 cm^{-1} which assigned to stretching vibration of the hydroxyl group, CH stretching, carbonyl groups in the free COOH group, and glucose carbonyl of cellulose, respectively. EC spectrum has

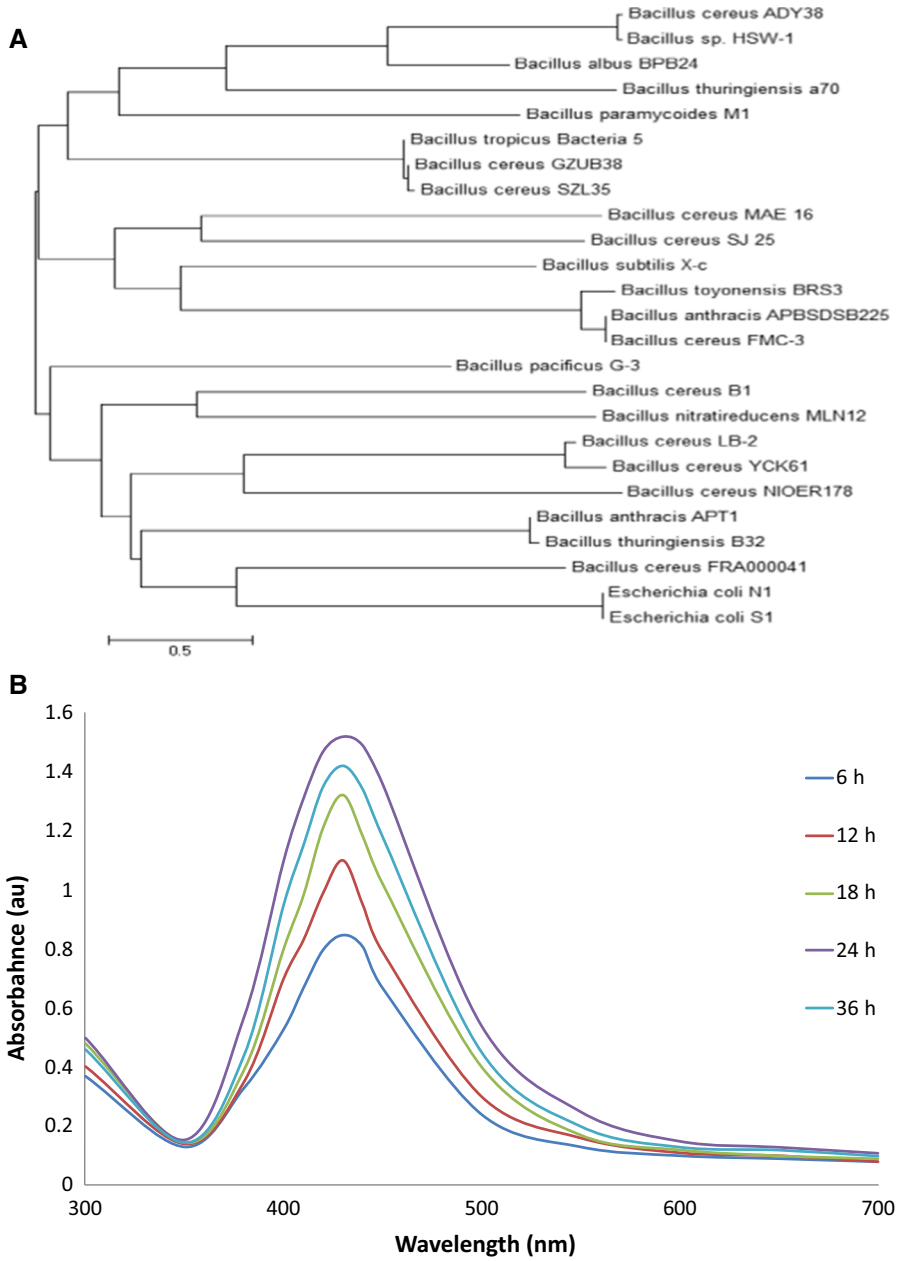

Fig. 1 **A** Neighbour-joining phylogenetic tree obtained by distance matrix analysis of 16S rRNA gene sequences, showing the position of strain MAE 16 among neighbors of *Bacillus spp*. **B** UV–vis absorption spectra of Ag-NPs synthesized by *Bacillus cereus* MAE 16 showing a peak at 430 nm.

shown a peak at 3660 cm^{-1} in which attributed to the stretching vibrations of OH group. The sharp peak at 2974 cm^{-1} and broad band at 2300 cm^{-1} were assigned for CH group stretching and H–C–H asymmetric and symmetric stretch of terminal CH_3 of primary ethyl group, respectively. The other bands at 1049, and 1370 cm^{-1} corresponded to C–O–C stretching and C–H bending, respectively.

On the other hand, the Ag-NC spectrum was observed the significant changes in the main band of native nanocomposite materials. The band of OH groups was observed at 3429 cm^{-1} which referred to high shift to low frequency of all polysaccharide components these informed that the interaction of Ag-NPs in nanocomposite involved via OH groups. Additionally, the CH starching vibration band was split to two small band at 2977 and 2925 cm^{-1}.

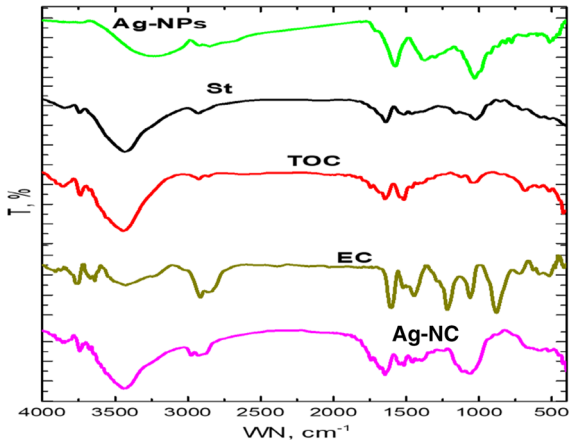

Fig. 2 FTIR of silver nanoparticles (Ag-NPs), starch (St), TEMPO oxidized cellulose (TOC), ethyl cellulose (EC), Ag-NPs loaded nanocomposite (Ag-NC).

However, the TEMPO band at 1746 cm^{-1} was assigned at is position without change as well as the band of glucose ring CO was split two to small bands at 1113 and 1059 cm^{-1} as result to incorporate of Ag ion. Inhere, the peak of Ag-NPs in main spectrum was shifted to higher frequency at 512 cm^{-1}. These observations were emphasized the incorporation of the three components with Ag-NPs.

XRD

The crystallographic pattern of Ag-NPs, St, TEMPO, EC and nanocomposite (Ag-NC) were carried out as shown in Fig. 3. The Ag-NPs pattern shows a typical crystallographic pattern with patterns at 36, 44, 64 and

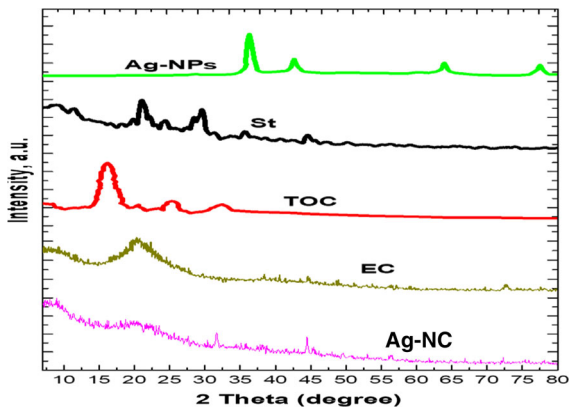

Fig. 3 Crystallographic of silver nanoparticles (Ag-NPs), Ag-NPs, starch (St), TEMPO oxidized cellulose (TOC), ethyl cellulose (EC), Ag-NPs loaded nanocomposite (Ag-NC).

78° corresponding to the (111), (200), (220) and (311) planes of silver were confirmed using standard powder diffraction data of the Joint Committee on Powder Diffraction Standards (JCPDS no. 04–0783). All peaks corresponded to a face centered cubic (fcc) symmetry (Basavegowda and Rok Lee 2013). On the other hand, all used polysaccharide were observed a typical XRD pattern. In addition, the composite was observed as polysaccharide pattern with some peaks for Ag-NPs. The peaks at 38° and 45° which shifted to high theta while bands at 63° and 75° were shifted to low theta.

Topography study

The topography study of Ag-NC was carried out using SEM, EDX and TEM. The SEM image and EDX as shown in Fig. 4. Fig. 4A illustrates Ag-NPs localized on the nanocomposite surface and aggregated in some positions and good disrupted in most locations. The EDX chart clarified the silver ion involved in the atomic content of nanocomposite. In addition, the TEM of neat Ag-NPs illustrated the nanoparticle in average size 15 nm (Fig. 4B). In this context, the nanocomposite images in low and high magnifications TEM for nanocomposite. The low magnification image showed clusters of polysaccharides doped with Ag-NPs. In addition, the high magnification image affirmed that the nanocomposite structure is belong nanoscale where the particles are low 100 nm as well as the Ag-NPs were determined clearly into nanocomposite particles. Besides, the diffraction pattern of nanocomposite was emphasized the crystalline structure of nanocomposite. These results may be due to incorporating the Ag-NPs into tertiary composite. The instrumental analysis confirmed that the preparation of tritely composite doped Ag-NPs was done and the sized of nanocomposite particles are less than 100 nm.

Antifungal activity

In the last two decades, composites based on cellulose, polysaccharides and metal nanoparticles were wildly used as antimicrobial activity to decrease bacterial and fungal infections (El-Naggar et al. 2020; Sureshkumar et al. 2010). In this study, our prepared tertiary nanocomposite which made of biosynthesized Ag-NPs, ethyl cellulose, TEMPO oxidized cellulose and starch was evaluated as antifungal towards *C. albicans*

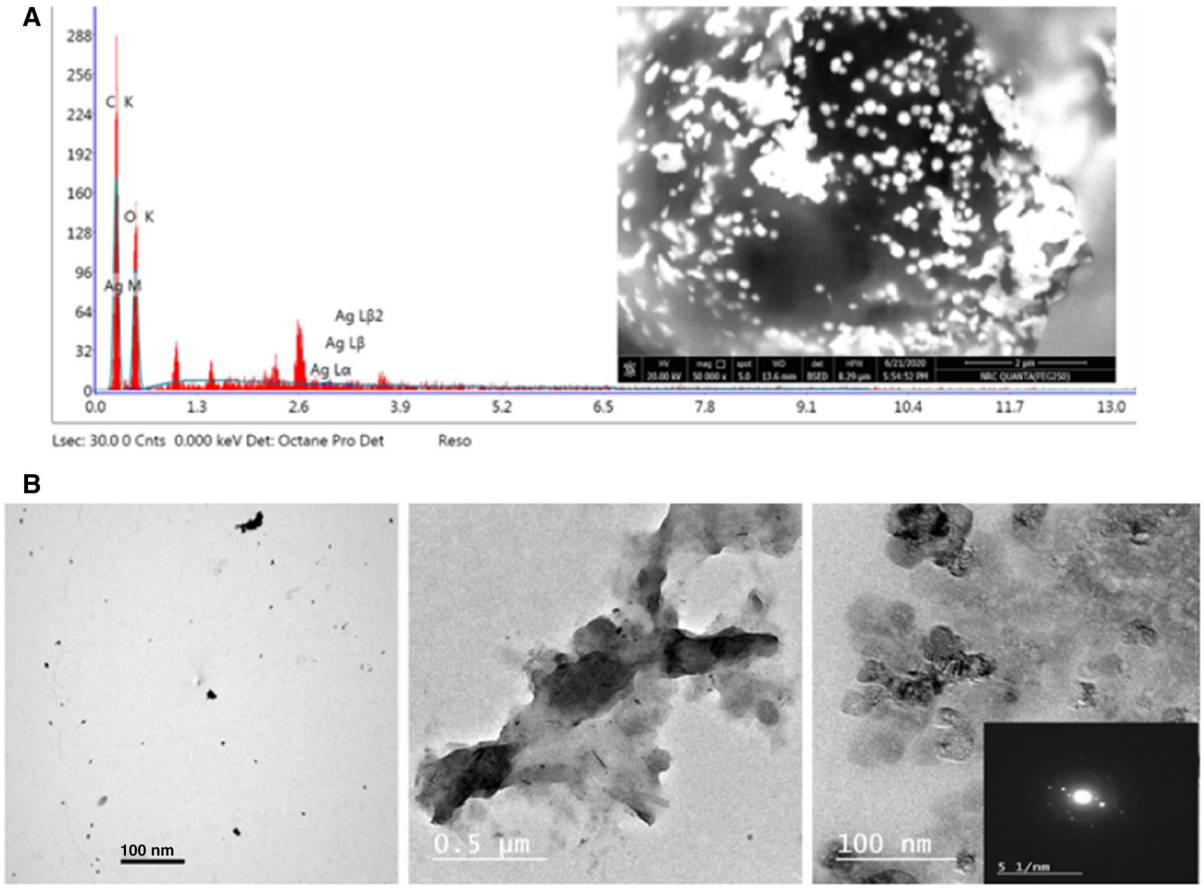

Fig. 4 SEM and EDX of Ag-NC (**A**) and TEM of AgNPs (left) and Ag-NC (middle and right) (**B**).

Table 1 Antifungal activities and MICs of Ag-NPs and Ag-NC

Tested fungal strain	Ag-NC		Ag-NPs		$AgNO_3$		Nystatin	
	IZ (mm) (10 mg/mL)	MIC (µg/mL)	IZ (mm) (10 mg/mL)	MIC (µg/mL)	IZ (mm) (10 mg/mL)	MIC (µg/mL)	IZ (mm) (10 mg/mL)	MIC (µg/mL)
A. flavus	30.07 ± 1.10	0.312	25.83 ± 0.76	0.625	0	ND	11.17 ± 0.76	10
A. terreus	30.97 ± 1.55	0.312	24.90 ± 1.35	1.25	0	ND	9.60 ± 0.36	10
A. fumigatus	26.00 ± 1.00	0.625	18.93 ± 1.10	2.5	0	ND	14.97 ± 0.55	5
A. niger	32.20 ± 1.71	0.156	28.10 ± 1.15	0.625	0	ND	11.50 ± 0.50	10
C. albicans	25.90 ± 0.85	1.25	24.67 ± 1.53	2.5	0	ND	12.67 ± 0.58	10

IZ inhibition zone, *ND* not detected

and *Aspergillus spp.* as shown in Table 1 and Fig. 5. Results revealed that, Ag-NC exhibited antifungal activity against tested *C. albicans* and the four strains of *Aspergillus.* The antifungal effects of Ag-NC were higher than Ag-NPs and nystatin. Inhibition zones of the Ag-NC against *C. albicans, A. niger, A. terreus, A. flavus* and *A. fumigatus* were 25.90 ± 0.85, 32.20 ± 1.71, 30.97 ± 1.55, 30.07 ± 1.10 and 26.00 ± 1.00, respectively. Meanwhile, inhibition zones of Ag-NPs were 24.67 ± 1.53, 28.10 ± 1.15,

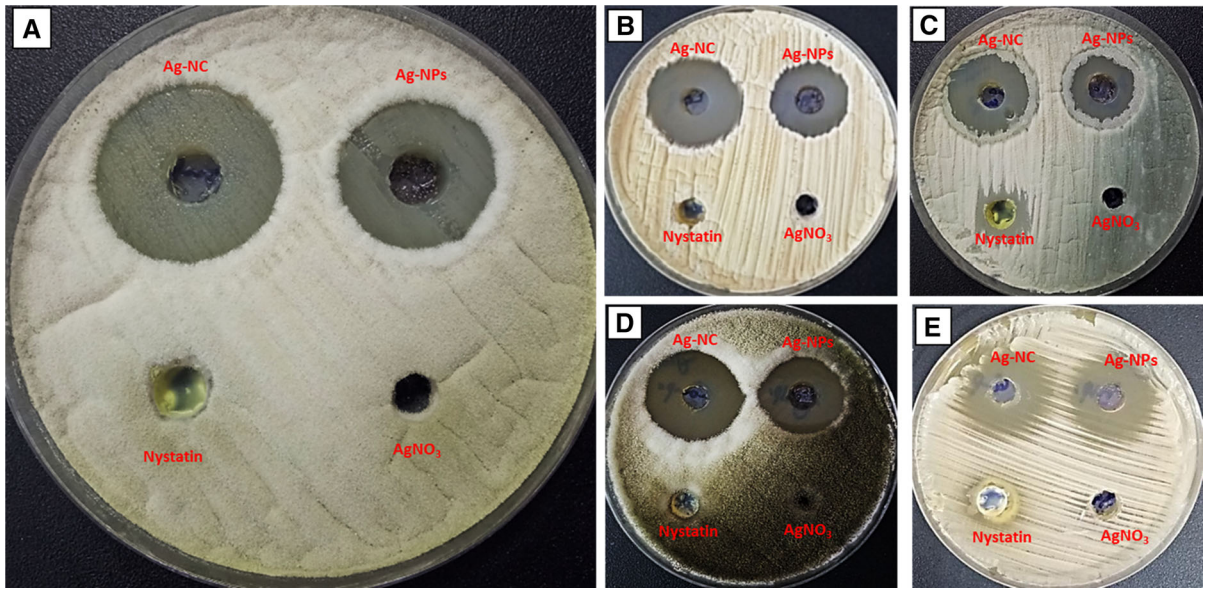

Fig. 5 Antifungal activity of Ag-NC and AgNPs against *A. flavus* RCMB 02782 (**A**), *A. terreus* RCMB 02574 (**B**), *A. fumigatus* RCMB 02568 (**C**), *A. niger* RCMB 02724 (**D**) *and C. albicans* ATCC 90028 (**E**). $AgNO_3$ and Nystatin were used as controls.

24.90 ± 1.35, 25.83 ± 0.76 and 18.93 ± 1.10 mm respectively. Silver nitrate solution did not show any antifungal activity against all tested fungal strains, confirming that reduction into nano-forms silver is beneficial in terms of antifungal activity. On the other hand, nystatin exhibited weak antifungal activity with inhibition zones of 12.67 ± 0.58, 11.50 ± 0.50, 9.60 ± 0.36, 11.17 ± 0.76 and 14.97 ± 0.55 mm, respectively against *C. albicans, A. niger, A. terreus, A. flavus* and *A. fumigatus*.

Moreover, MICs values of Ag-NC, Ag-NPs and nystatin were evaluated as shown in Table 1. Results illustrated that, MIC of Ag-NC towards all tested fungal strains was better than MIC of Ag-NPs and nystatin. MICs of Ag-NC towards *C. albicans, A. niger, A. terreus, A. flavus* and *A. fumigatus* were 1.25, 0.156, 0.312, 0.312 and 0.625 mg/ml, respectively. Additionally, *A. niger* was the highest affected by the nanocomposite, while *C. albicans* was the lowest one. Moreover, MICs of Ag-NPs against *C. albicans, A. niger, A. terreus, A. flavus* and *A. fumigatus* were 2.5, 0.625, 1.25, 0.625 and 2.5 mg/ml, respectively. On the other hand, MICs of nystatin toward all tested fungal strains were in range 5–10 mg/ml. Eventually, low concentrations of Ag-NC (0.312–1.25 mg/ml) and Ag-NPs (0.625–2.5 mg/ml) exhibited promising antifungal activity toward *C. albicans* and *Aspergillus spp*. which cause invasive candidiasis and aspergillosis respectively. In accordance with our results, (Ashrafi et al. 2020) evaluated the antifungal activity of Ag-NPs based on chitosan nanocomposite, and found MIC was 0.438 mg/ml against *C. albicans*.

Antibacterial activity

In this study, Ag-NC and biosynthesized Ag-NPs were evaluated towards two-gram negative bacteria strains (*E. coli* ATCC 25922 and *P.* aeruginosa ATCC 27853) and two-gram positive bacteria strains (*S. aureus* ATCC23235 and *B. subtilis* ATCC23857) by agar-well diffusion method. The antibacterial activities of these nanoparticles were evaluated by determining the presence of inhibition zones as shown in Table 2 and Fig. 6. Inhibition zones of the designed nanocomposite against *E. coli, P. aeruginosa*, S. aureus and *B. subtilis* were 31 ± 0.42, 29 ± 1.2, 26 ± 1.1 and 22 ± 1.3, respectively. Results of antibacterial activity indicated that Ag-NC suspension significantly suppressed growth of tested bacterial gram positive and gram negative as compared with non-treated control and Ag-NPs. The largest antibacterial activity was observed by Ag-NC suspension at 50 µg/ml, while exhibited the maximum diameter of the inhibition zone (31 ± 0.42 mm)

Table 2 Antibacterial activities and MICs of Ag-NC and AgNPs.

Tested bacterial strain	Ag-NC		Ag-NPs		AgNO3		Amikacin	
	IZ (mm) (50 µg/mL)	MIC (µg/mL)	IZ (mm) (50 µg/mL)	MIC (µg/mL)	IZ (mm) (50 µg/mL)	MIC (µg/mL)	IZ (mm) (50 µg/mL)	MIC (µg/mL)
Staphylococcus aureus ATCC23235	26 ± 1.1	40	22 ± 0.42	80	0	ND	24 ± 0.17	160
Escherichia coli ATCC 25922	31 ± 0.42	20	26 ± 0.15	80	0	ND	25 ± 0.37	80
Bacillus subtilis ATCC23857	22 ± 1.3	40	18 ± 0.28	160	0	ND	26 ± 0.25	80
Pseudomonas aeruginosa ATCC 27853	29 ± 1.2	40	24 ± 0.82	160	0	ND	23 ± 0.27	80

IZ inhibition zone, *ND* not detected

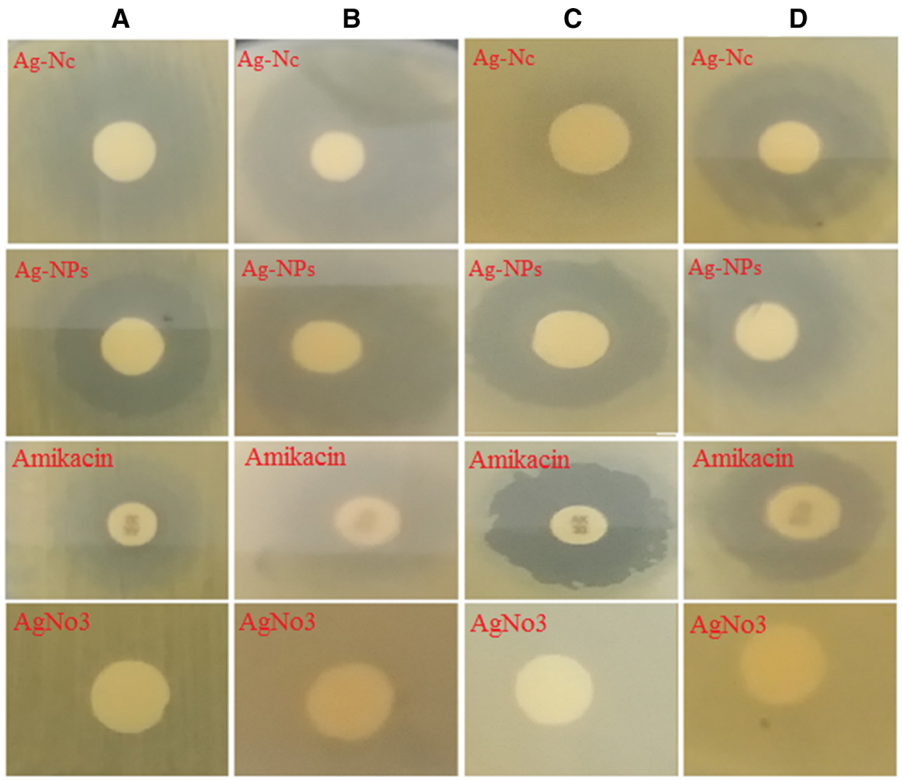

Fig. 6 Antibacterial activity of Ag-NC and AgNPs against *Staphylococcus aureus* ATCC23235 (**A**), *Escherichia coli* ATCC 25922 (**B**), *A Bacillus subtilis* ATCC23857 (**C**), and *Pseudomonas aeruginosa* ATCC 27853. $AgNO_3$ and Amikacin were used as controls.

against *E. coli*. Also, Antibacterial activities of the Ag-NC and Ag-NPs were determined by means of a standard dilution assay which enables to state the minimum concentration of the tested compound needed for a growth inhibition of tested bacteria. For testing of antimicrobial activity, we prepared concentrated aqueous dispersion of the biosynthesized Ag-NPs, the final mass concentrations of silver present in such concentrated dispersions of the studied nanocomposites corresponded to the values of concentrations (160–10 µg/ml). In vitro minimum inhibitory concentration (MIC) results revealed that Ag-NC significantly inhibited the growth of tested microorganism after 48 h of incubation. Indeed, the inhibitory effect on bacterial growth was increased with the increase of the concentration of Ag-NC at four different

concentrations (10, 20, 40, 80 and 160 µg/ml) caused (33.15%, 41.19%, 56.51%, 92.12%) reduction of bacterial growth respectively. Hence, the result revealed that Ag-NC has great potential in controlling the growth of gram positive and gram-negative bacteria. Final, The MIC values acquired for Ag-NC fall into range from 20 to 40 µg/mL as shown in Table 2. Taking into account the acquired results, prepared Ag-NC do not practically lose their antimicrobial activity. Likewise, iron oxide nanoparticles maintain their magnetic properties after loading into a nanocomposite. This is important from the point of view of the application potential of these nanocomposites in medical field (Cobos et al. 2020; Farag et al. 2020). Overall, our prepared Ag-NC exhibited antimicrobial activities higher than Ag-NPs alone due to that Ag-NPs in the composite is functionalized with TEMPO oxidized cellulose, starch and ethyle cellulose where increased the availability through spatial distribution (Tamayo et al. 2019).

In vitro cytotoxicity assay

The potential cytotoxic effect of Ag-NC and Ag-NPs was evaluated against Vero cells to determine the maximum non-toxic dose (MNTD). As shown in Fig. 7A, the viability of Vero cells was much more better when treated with Ag-NC than free Ag-NPs. The viability of Vero cells was more than 95% with concentrations of 3.12 and 6.25 µg/mL for Ag-NPs and 3.12, 6.25, and 12.5 µg/mL for Ag-NC, indicating that Ag-NC is less toxic against Vero cells. The cytotoxicity against Vero cell line was observed when the concentrations was higher than 6.25 µg/mL and 12.5 µg/mL for Ag-NPs and Ag-NC, respectively, considering these concentrations as MNTD. The viability (%) of Vero cells were 97.4 ± 1.6, 90.3 ± 23, 78.3 ± 2.8, 61.7 ± 2.8, 37.9 ± 2.3, 13,9 ± 1.6, 9.25 ± 1.1 and 4.9 ± 0.5 corresponding to Ag-NPs concentrations 6.25, 12.5, 25, 50, 100, 200, 400 and 800 µg/mL, respectively. Meanwhile, the viability (%) of Vero cells were 98.6 ± 1.8, 89.5 ± 4.3, 77.3 ± 3.6, 68.2 ± 3.3, 45.8 ± 2.5, 33.3 ± 2.4, and 9.3 ± 1.5 to Ag-NC concentrations 12.5, 25, 50, 100, 200, 400 and 800 µg/mL, respectively. MTT assay exhibited that the cytotoxicity increased with increasing nanoparticles concentrations, with the 50% cytotoxic concentration (CC50) at 69.3 and 171.4 µg/mL for Ag-NPs and Ag-NC, respectively. Microscopic observations exhibited dose-dependent morphological changes in treated Vero cells (Fig. 7B). Overall, cytotoxicity of Ag-NPs against Vero cells was decreased by incorporation into nanocomposite. With concentration over MNTD, Vero cells turned on morphological abnormalities and became more floated, shrunken and rounded (Shehabeldine et al. 2021b).

Antiviral activity

To investigate the antiviral effects of Ag-NPs and Ag-NC, viruses (HSV-1, Adeno, and CoxB2) were pretreated with either MNTD, 0.5 × MNTD, or 0.25 × MNTD of each compound and were assessed by MTT assay in Vero cell line (Fig. 8). Any cytopathogenic effect (CPE) or any structural changes in Vero cells were recorded by inverted microscope as sign of viral invasion. No CPE was found in control group (uninfected Vero cells), but cells infected with HSV-1, Adeno, or CoxB2 have shown irregular outline, cytoplasmic projections, intense cytoplasmic vacuolization, dense lysosomes, myelin figures, disintegrated nuclear membrane, and unseen nuclei (Fig. 8A). In contrast, when HSV-1, Adeno, and CoxB2 were pre-treated with either Ag-NPs (6.25 µg/mL) or Ag-NC (12.5 µg/mL) for 1 h prior to infection, no significant CPE was found (Fig. 5A). Following incubation of HSV-1, Adeno, and CoxB2 with either Ag-NPs (1.56, 3.12, 6.25 µg/mL) or Ag-NPs-nanocomposite (3.12, 6.25, 12.5 µg/mL) for one hour, Vero cells exhibited significant dose-dependent reductions in viruses replications (Fig. 8B). The dose of 6.25 µg/mL Ag-NPs was the most effective in all tested viruses with a decrease of 61.7 ± 6.6, 20.1 ± 1.6, and 11.9 ± 1.2% of replications of HSV-1, CoxB2, and Adeno, respectively in Vero cells. Same dose (6.25 µg/mL) for Ag-NC showed modest antiviral activity in Vero cells (12.9 ± 5.6, 9.1 ± 5.2, and 1.8 ± 1.6% against HSV-1, CoxB2, and Adeno, respectively). The dose of 12.50 µg/mL Ag-NPs was the most effective against all tested viruses with a decrease of 37.3, 22.7, and 4.6% of replications of HSV-1, CoxB2, and Adeno, respectively in Vero cells. The results revealed both Ag-NPs and Ag-NC have a varied antiviral effect and both were much more active against HSV-1 followed by CoxB2, and finally Adeno. In contrast to antibacterial and antifungal activities of Ag-NC, Ag-NC has shown

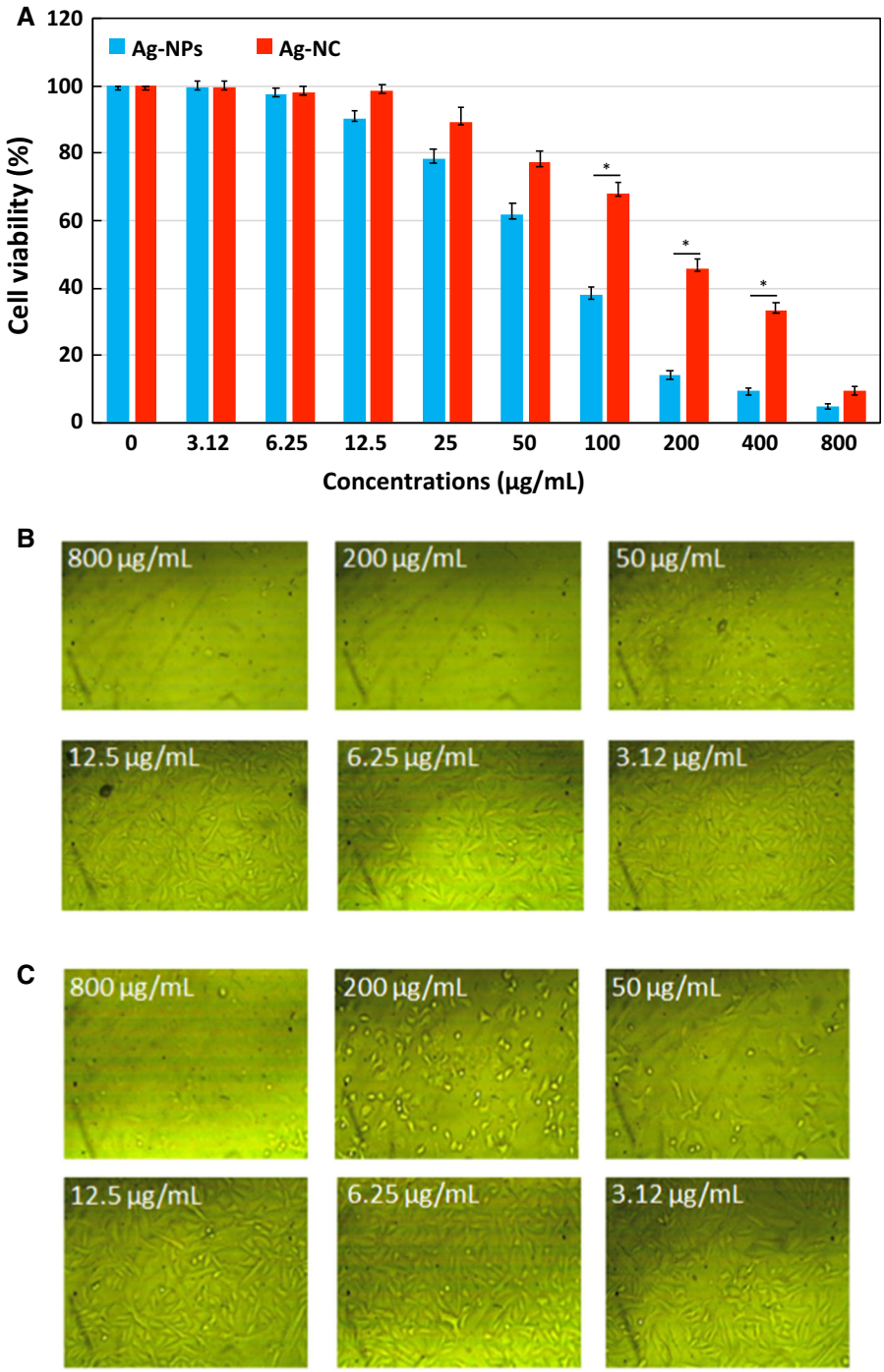

Fig. 7 The cytotoxicity effect of free silver nanoparticles (Ag-NPs) and Ag-NPs loaded nanocomposite (Ag-NC) on Vero cells for 24 h. (**A**) The viability percent of Vero cells treated with either AgNPs or Ag-NC at indicated concentrations for 24 h as determined by MTT assay. Significance is indicated in figures, *$p < 0.05$, and otherwise not mentioned is not significant. Morphological changes of Vero cells treated with AgNPs (**B**) and Ag-NC (**C**) (×10 magnification). Each experiment performed in triplicate and the error bar represents the standard deviation.

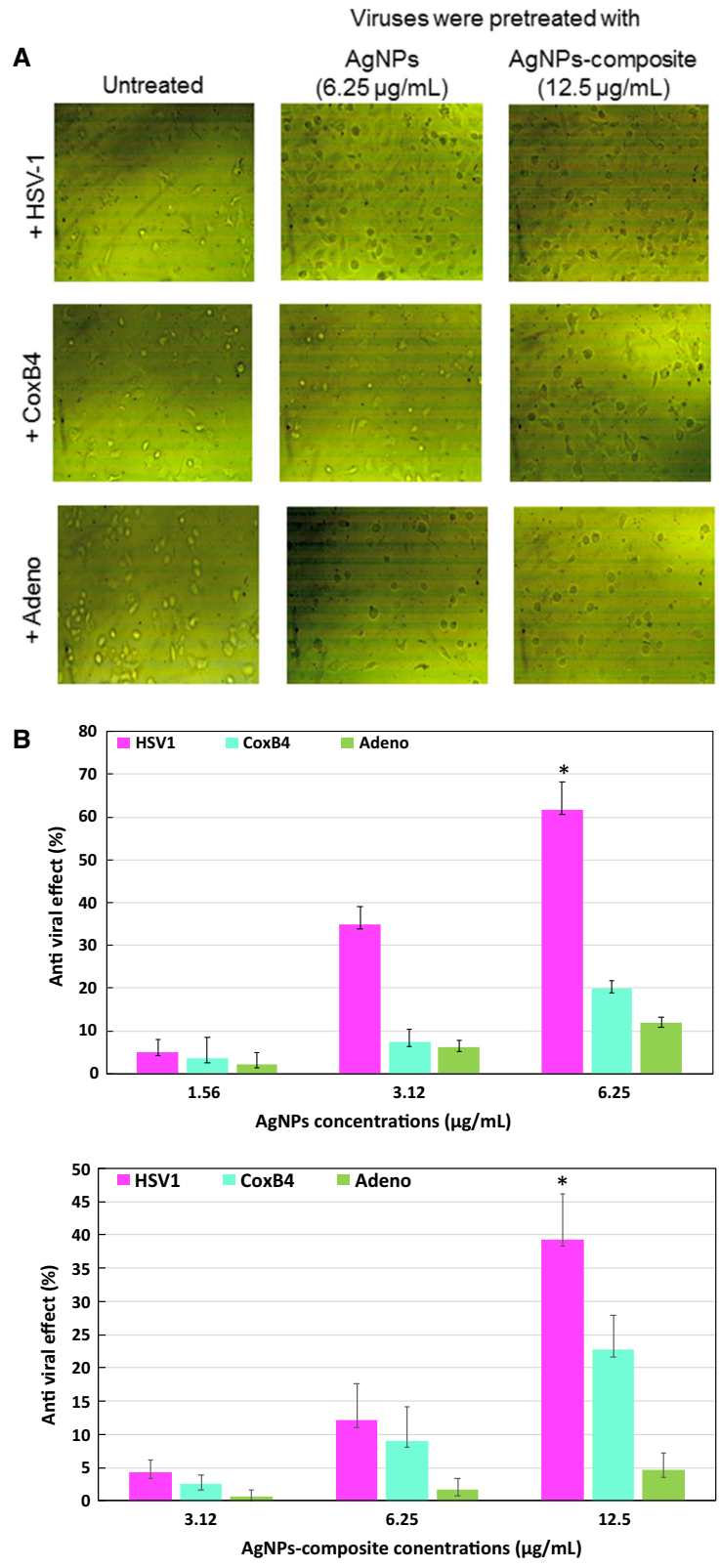

Fig. 8 The antiviral effect of free silver nanoparticles (Ag-NPs) and Ag-NPs loaded nanocomposite (Ag-NC) against Herpes simplex virus (HSV-1), Adenovirus (Adeno) and Coxsackie B virus 2 (CoxB2) in Vero cell line. Overnight-grown Vero cells in were infected with either HSV-1, Adeno, or CoxB2 that pre-treated with AgNPs (1.56, 3.12, 6.25 µg/mL) or AgNPs-composite (3.12, 6.25, 12.5 µg/mL) for 1 h prior to infection. After incubation for for 24 h, cells were washed and incubated for 48 h. Next, cellular viability was detected at OD_{560} nm and the antiviral effect was observed by inverted microscope. (**A**) The antiviral effect CPE of Vero cells infected with untreated or treated (MNTD of AgNPs or Ag-NC) HSV-1, Adeno, or CoxB2 (×10 magnification). (**B**) The antiviral effect of AgNPs and AgNPs-composite was calculated as percentage relative to control (untreated) infected Vero cells in the range of maximum non-toxic dose (MNTD). Significance is indicated in figures, *$p < 0.05$, and otherwise not mentioned is not significant

lower antiviral activity compared to free Ag-NPs. This decreased antiviral effect of Ag-NC could be attributed to the lower uptake of Ag-NC by Vero cells and to the lower concentrations of Ag-NPs in nanocomposite compared to free Ag-NPs. Ag-NPs can inhibit the viral multiplication inside the host cells by preventing the replication or blocking the entry of virus particles inside the host cells. However, the mechanism behind the antiviral effect of Ag-NPs has been proposed to interfere with viral replication by two separate mechanisms, (1) Ag-NPs can bind to sulfur-containing residues on surface glycoproteins of virus, blocking of virus-host cell binding and penetration and thus will leaving the virus in the extracellular space where it is unable to propagate (Morris et al. 2019), (2) Ag-NPs can cross the cell membrane and interacting with viral factors and double strand DNA, and thus blocking viral replication and the proper assembly of viral progeny (Galdiero et al. 2011). Overall, incorporation of Ag-NPs into nanocomposite is very effective as antimicrobial activity as well as antiviral activity.

Conclusion

In the current study, a tertiary nanocomposite made of starch, TEMPO oxidized cellulose and ethyl cellulose was loaded by biosynthesized Ag-NPs through ecofriendly method. The prepared Ag-NPs loaded nanocomposite (Ag-NC) was fully characterized using FT-IR, XRD, SEM, EDX and TEM. Biological applications were carried out as antibacterial, antifungal and antiviral activity. The results suggest that the use of Ag-NPs together with TEMPO oxidized cellulose, starch and ethyl cellulose results in a better antimicrobial material. Moreover, Loading of Ag-NPs into nanocomposites will decrease the cytotoxicity of Ag-NPs against normal Vero cells. Data confirm that Ag-NPs loaded nanocomposites is a potential new antimicrobial material.

Author contribution MH: Conceptualization, data curation, investigation, methodology (Preparation and characterization of nanocomposite), writing review and editing: MAE: Conceptualization, data curation, investigation, methodology (Isolation and identification of the bacterial isolate; biosynthesis and characterization of Ag-NPs; Antiviral activity), writing review and editing; AMS: Conceptualization, data curation, investigation, methodology (Antibacterial and antiviral activity), writing review and editing; AHH: Conceptualization, data curation, investigation, methodology (Antifungal and antiviral activity), writing review and editing.

Declarations

Competing interest The authors state no potential conflict of interest.

References

Abo-State MA, Mahdy HM, Ezzat SM, Abd El Shakour EH, El-Bahnasawy MA (2012) Antimicrobial resistance profiles of Enterobacteriaceae isolated from Rosetta Branch of river Nile, Egypt. World Appl Sci J 19(9):1234–1243

Abu-Elghait M, Hasanin M, Hashem AH, Salem SS (2021) Ecofriendly novel synthesis of tertiary composite based on cellulose and myco-synthesized selenium nanoparticles: characterization, antibiofilm and biocompatibility. Int J Biol Macromol 175:294–303

Ashrafi M, Bayat M, Mortazavi P, Hashemi SJ, Meimandipour A (2020) Antimicrobial effect of chitosan–silver–copper nanocomposite on Candida albicans. J Nanostruct Chem 10:87–95

Balouiri M, Sadiki M, Ibnsouda SK (2016) Methods for in vitro evaluating antimicrobial activity: a review. J Pharm Anal 6:71–79

Basavegowda N, Lee YR (2013) Synthesis of silver nanoparticles using Satsuma mandarin (Citrus unshiu) peel extract: a novel approach towards waste utilization. Mater Lett 109:31–33

Bhavya G, Belorkar SA, Mythili R, Geetha N, Shetty HS, Udikeri SS, Jogaiah S (2021) Remediation of emerging environmental pollutants: a review based on advances in the uses of eco-friendly biofabricated nanomaterials. Chemosphere 275:129975

Bongomin F, Gago S, Oladele RO, Denning DW (2017) Global and multi-national prevalence of fungal diseases—estimate precision. J Fungi 3(4):57

Campoy S, Adrio JL (2017) Antifungals. Biochem Pharmacol 133:86–96

Chang Y-L, Yu S-J, Heitman J, Wellington M, Chen Y-L (2017) New Facets Antifungal Ther Virul 8:222–236

Chen N, Zheng Y, Yin J, Li X, Zheng C (2013) Inhibitory effects of silver nanoparticles against adenovirus type 3 in vitro. J Virol Methods 193(2):470–477

Cobos M, De-La-Pinta I, Quindós G, Fernández MJ, Fernández MD (2020) Graphene oxide–silver nanoparticle nanohybrids: synthesis, characterization, and antimicrobial properties. Nanomaterials 10(2):376

Dacrory S, Hashem AH, Hasanin M (2021) Synthesis of cellulose based amino acid functionalized nano-biocomplex: characterization, antifungal activity, molecular docking and hemocompatibility. Environ Nanotechnol Monit Manag 15:100453

Dhingra S, Rahman NAA, Peile E, Rahman M, Sartelli M, Hassali MA et al (2020) Microbial resistance movements: an overview of global public health threats posed by

antimicrobial resistance, and how best to counter. Front Public Health 8:531
Elbahnasawy MA, Farag MM, Mansour MT, El-Ghamery AA (2020) Cloning, expression and nanodiscs assemble of recombinant HIV-1 gp41. Microbial Pathog 138:103824
Elbahnasawy MA, ElSayed EE, Azzam MI (2021a) Newly isolated coliphages for bio-controlling multidrug resistant Escherichia coli strains. Environ Nanotechnol Monitor Manag 16:100542
Elbahnasawy MA, Shehabeldine AM, Khattab AM, Amin BH, Hashem AH (2021b) Green biosynthesis of silver nanoparticles using novel endophytic Rothia endophytica: characterization and anticandidal *activity*. J Drug Deliv Sci Technol 62:102401
El-Naggar ME, Hasanin M, Youssef AM, Aldalbahi A, El-Newehy MH, Abdelhameed RM (2020) Hydroxyethyl cellulose/bacterial cellulose cryogel dopped silver@ titanium oxide nanoparticles: antimicrobial activity and controlled release of Tebuconazole fungicide. Int J Biol Macromol 165:1010–1021
El-Nahhal IM, Salem J, Anbar R, Kodeh FS, Elmanama A (2020) Preparation and antimicrobial activity of ZnO-NPs coated cotton/starch and their functionalized ZnO-Ag/cotton and Zn (II) curcumin/cotton materials. Sci Rep 10(1):1–10
Elsayed H, Hasanin M, Rehan M (2021) Enhancement of multifunctional properties of leather surface decorated with silver nanoparticles (Ag NPs). J Mol Struct 1234:130130
El-Zayat MM, Eraqi MM, Alrefai H, El-Khateeb AY, Ibrahim MA, Aljohani HM et al (2021) The antimicrobial, antioxidant, and anticancer activity of greenly synthesized selenium and zinc composite nanoparticles using Ephedra aphylla extract. Biomolecules 11(3):470
Ezzat SM, Mahdy HM, El-Shakour A, El-Bahnasawy MA (2014) The effect of ionizing radiation on multi-drug resistant *Pseudomonas aeruginosa* isolated from aquatic environments in Egypt. Microbiol Res J 4(8):856–868
Farag MM, Ahmed MM, Abdallah NM, Swieszkowski W, Shehabeldine AM (2020) The combined antibacterial and anticancer properties of nano Ce-containing Mg-phosphate ceramic. Life Sci 257:117999
Galdiero S, Falanga A, Vitiello M, Cantisani M, Marra V, Galdiero M (2011) Silver nanoparticles as potential antiviral agents. Molecules 16(10):8894–8918
Hamouda T, Ibrahim HM, Kafafy HH, Mashaly HM, Mohamed NH, Aly NM (2021) Preparation of cellulose based wipes treated with antimicrobial and antiviral silver nanoparticles as novel effective high-performance coronavirus fighter. Int J Biol Macromol 181:990
Hasanin MS, Moustafa GO (2020) New potential green, bioactive and antimicrobial nanocomposites based on cellulose and amino acid. Int J Biol Macromol 144:441–448
Hasanin M, Al Abboud MA, Alawlaqi MM, Abdelghany TM, Hashem AH (2021a) Ecofriendly synthesis of biosynthesized copper nanoparticles with starch-based nanocomposite: antimicrobial, antioxidant, and anticancer activities. Biol Trace Elem Res. https://doi.org/10.1007/s12011-021-02812-0
Hasanin M, Hashem AH, Lashin I, Hassan SAM (2021b) In vitro improvement and rooting of banana plantlets using antifungal nanocomposite based on myco-synthesized copper oxide nanoparticles and starch. Biomass Convers Bioref 2:89. https://doi.org/10.1007/s13399-021-01784-4
Hashem AH, Suleiman WB, Abu-elreesh G, Shehabeldine AM, Khalil AMA (2020) Sustainable lipid production from oleaginous fungus *Syncephalastrum racemosum* using synthetic and watermelon peel waste media. Bioresour Technol Rep 12:100569. https://doi.org/10.1016/j.biteb.2020.100569
Hashem AH, Abdelaziz AM, Askar AA, Fouda HM, Khalil AMA, Abd-Elsalam KA, Khaleil MM (2021a) Bacillus megaterium-mediated synthesis of selenium nanoparticles and their antifungal activity against Rhizoctonia solani in Faba Bean Plants. J Fungi 7:195
Hashem AH, Khalil AMA, Reyad AM, Salem SS (2021b) Biomedical applications of mycosynthesized selenium nanoparticles using *Penicillium expansum* ATTC 36200. Biol Trace Elem Res 199:3998
GAFFI GP How 150 people die every hour from fungal infection while the world turns a blind eye. *Global Action Fund for Fungal Infections* (GAFFI), 2013
Jeremiah SS, Miyakawa K, Morita T, Yamaoka Y, Ryo A (2020) Potent antiviral effect of silver nanoparticles on SARS-CoV-2. Biochem Biophys Res Commun 533(1):195–200
Jogaiah S, Kurjogi M, Abdelrahman M, Hanumanthappa N, Tran L-SP (2019) Ganoderma applanatum-mediated green synthesis of silver nanoparticles: Structural characterization, and in vitro and in vivo biomedical and agrochemical properties. Arab J Chem 12:1108–1120
Khalil AMA, Hashem AH (2018) Morphological changes of conidiogenesis in two aspergillus species. J Pure Appl Microbiol 12:2041–2048
Konappa N et al (2021) Ameliorated antibacterial and antioxidant properties by trichoderma harzianum mediated green synthesis of silver nanoparticles. Biomolecules 11:535
Maduray K, Parboosing R (2020) Metal nanoparticles: a promising treatment for viral and arboviral infections. Biol Trace Elem Res 199:1–18
Makvandi P, Wang CY, Zare EN, Borzacchiello A, Niu LN, Tay FR (2020) Metal-based nanomaterials in biomedical applications: antimicrobial activity and cytotoxicity aspects. Adv Funct Mater 30(22):1910021
Morris D, Ansar M, Speshock J, Ivanciuc T, Qu Y, Casola A, Garofalo RP (2019) Antiviral and immunomodulatory activity of silver nanoparticles in experimental RSV infection. Viruses 11(8):732
Nayak S, Bhat MP, Udayashankar A, Lakshmeesha T, Geetha N, Jogaiah S (2020) Biosynthesis and characterization of Dillenia indica-mediated silver nanoparticles and their biological activity. Appl Organometall Chem 34:e5567
Schmiedel Y, Zimmerli S (2016) Common invasive fungal diseases: an overview of invasive candidiasis, aspergillosis, cryptococcosis, and *Pneumocystis pneumonia*. Swiss Med Wkly 146:14281
Shehabeldine A, Hasanin M (2019) Green synthesis of hydrolyzed starch–chitosan nano-composite as drug delivery system to gram negative bacteria. Environ Nanotechnol Monit Manag 12:100252
Shehabeldine AM, Ashour RM, Okba MM, Saber FR (2020) Callistemon citrinus bioactive metabolites as new

inhibitors of methicillin-resistant Staphylococcus aureus biofilm formation. J Ethnopharmacol 254:112669

Shehabeldine A, El-Hamshary H, Hasanin M, El-Faham A, Al-Sahly M (2021a) Enhancing the antifungal activity of griseofulvin by incorporation a green biopolymer-based nanocomposite. Polymers 13(4):542

Shehabeldine AM, Elbahnasawy MA, Hasaballah AI (2021b) Green phytosynthesis of silver nanoparticles using echinochloa stagnina extract with reference to their antibacterial, cytotoxic, and larvicidal activities. BioNanoScience, pp1–13.

Singh D, Rathod V, Ninganagouda S, Herimath J, Kulkarni P (2013) Biosynthesis of silver nanoparticle by endophytic fungi *Pencillium* sp. isolated from *Curcuma longa* (turmeric) and its antibacterial activity against pathogenic gram negative bacteria. J Pharm Res 7:448–453. https://doi.org/10.1016/j.jopr.2013.06.003

Sureshkumar M, Siswanto DY, Lee C-K (2010) Magnetic antimicrobial nanocomposite based on bacterial cellulose and silver nanoparticles. J Mater Chem 20:6948–6955

Tamayo L, Palza H, Bejarano J, Zapata PA (2019) Polymer composites with metal nanoparticles: synthesis, properties, and applications. In: Polymer composites with functionalized nanoparticles. Elsevier, pp 249–286

Xue Y, Chen S, Yu J, Bunes BR, Xue Z, Xu J et al (2020) Nanostructured conducting polymers and their composites: synthesis methodologies, morphologies and applications. J Mater Chem C 8(30):10136–10159

Yaqoob AA, Umar K, Ibrahim MNM (2020) Silver nanoparticles: various methods of synthesis, size affecting factors and their potential applications—a review. Appl Nanosci 10(5):1369–1378

Youssef AM, Hasanin MS, Abd El-Aziz ME, Turky GM (2021) Conducting chitosan/hydroxylethyl cellulose/polyaniline bionanocomposites hydrogel based on graphene oxide doped with Ag-NPs. Int J Biol Macromol 167:1435–1444